Dopant induced ablation of poly(methyl methacrylate) at 308 nm

T. Lippert
Los Alamos National Laboratory, CST-6, MS J 585, Los Alamos, New Mexico 87545

R. L. Webb
Department of Physics, Pacific Union College, Angwin, California 94508

S. C. Langford and J. T. Dickinson[a)]
Department of Physics, Washington State University, Pullman, Washington 99164-2814

(Received 8 July 1998; accepted for publication 23 October 1998)

Poly(methyl methacrylate) (PMMA) is highly resistant to laser ablation at 308 nm. Either very high fluences or absorbing dopants must be used to ablate PMMA efficiently at this wavelength. We investigate two dopants, pyrene and a common solvent, chlorobenzene, using time-of-flight mass spectroscopy. Both compounds improve the ablation characteristics of PMMA. For both dopants, the first step in ablation is an incubation process, in which absorption at 308 nm increases due to the production of C═C bonds along the polymer backbone. Incubation at 308 nm is similar to that observed for shorter ultraviolet wavelengths in previous studies. The principal ablation products and their corresponding temperatures are consistent with a photothermal ablation mechanism. © *1999 American Institute of Physics.* [S0021-8979(99)04703-9]

I. INTRODUCTION

The laser ablation of poly(methyl methacrylate) (PMMA) has been extensively studied due to its usefulness in lithography, semiconductor packaging, and medical applications.[1] Until recently, the short lifetime of optical components in the far ultraviolet (UV) has limited high through-put industrial applications to wavelengths $\geqslant$308 nm. However, PMMA is essentially transparent these wavelengths. The first significant absorption band of PMMA is the n-Π^* singlet of the ester group ($COOCH_3$), with an extinction coefficient of 45–50 (1 mol^{-1} cm^{-1}) at 220–230 nm.[2] Therefore most ablation of undoped PMMA is performed at shorter excimer wavelengths. At 308 nm PMMA is often doped with organic dyes to increase absorption.

At UV wavelengths below 260 nm, the principle ablation mechanisms appear to be photochemical. At 193 nm, the main product is the monomer, MMA (methyl methacrylate, yield ~18%), attributed to a one-photon photochemical process. Other products include C_2, assigned to a multiphoton process, CO_2, and low molecular weight PMMA fragments ($M_n<2500$).[3] At high fluences (high energy density per unit area per pulse), 248 nm irradiation produces much less monomer (yield$<$1%);[3] PMMA fragments with $M_n\sim2500$ dominate. However, at lower fluences, time-of-flight mass spectrometry (TOF-MS) reveals only minor amounts of high M_w products during irradiation at 248 nm.[4] Because thermal decomposition [e.g., by infrared (IR) laser irradiation at 1064 nm] yields only the monomer as a product,[5] it has been suggested that UV irradiation is a novel tool to generate bond scissions in organic solids.

At UV wavelengths above 260 nm, the ablation mechanism is more complex, yielding principally MMA, CO, and CO_2.[6,7] At 266 nm, the MMA intensity increases with fluence in a manner consistent with pyrolysis.[8,9] At 308 nm (ionizing the fragments at 193/248 nm), a threshold fluence of ~200 mJ/cm^2/pulse was determined from log-log plots of intensity versus fluence. A photothermal mechanism with product temperature of about 600 K was proposed. Higher M_w products were assigned to a MMA dimer.[10,11]

As the laser wavelength decreases from the IR to the UV, thermal decomposition becomes less and less important. At 1064 nm (with an IR dye to convert the laser energy into heat)[12] ablation temperatures of ~550 K were calculated—consistent with the thermal decomposition of PMMA.[13] At 193 nm, MMA was emitted with kinetic energies of 0.2–0.4 eV—attributed to a photochemical decomposition mechanism.[14] Even at 248 nm, the product kinetic energies were shown to be high: CH kinetic energies in the plume of ~0.4 eV.[15] Photochemical processes are still important at wavelengths longer than 260 nm, as evidenced by the presence of methyl formate (MMA was eliminated as a source).[15] Photothermal models[16] of ablation at wavelengths between 248 and 351 nm have displayed variable agreement with data suggesting the need for further studies.

An especially important feature of PMMA ablation, especially at wavelengths longer than 193 nm, is the so called incubation effect—an increase in product intensities with increasing number of laser pulses. Incubation is normally observed in polymers with absorptivities of less than 4000 cm^{-1}, and is accompanied by an increase in absorptivity.[17] Transient absorption changes have been observed in PMMA after irradiation at 193, 222, and 248 nm.[18] At 248 nm, an increase of the refractive index was also detected.[19] Permanent increases in absorptivity after irradiation at 193 nm have been observed and assigned to chemical changes in the polymer.[20] Fourier transform infrared (FTIR) spectroscopy after irradiation at 248 nm revealed C═C and C≡C, the latter due to occluded carbon monoxide.[21] Micro-Raman

a)Electronic mail: jtd@wsu.edu

studies after irradiation at 248 nm showed formation of conjugated structures (C═C-C═C units) and isolated C═C units,[22] originating from photolysis of the ester side chain. Effective etching at 308 nm has been demonstrated after incubation with continuous wave (cw) UV light[21] or with simultaneous irradiation at 193 nm.[23]

Time-of-flight mass spectroscopy during irradiation at 248 nm reveals a steady ''background'' emission at low masses ($\leqslant$60, e.g., CO_2, CH_3OH, $HCOOCH_3$).[5] These masses are consistent with photochemical scission of ester side chains, yielding low M_w products and forming C═C double bonds along the polymer backbone. During steady state ablation (where emission remains nearly constant from pulse-to-pulse), low M_w fragments ($<$150 amu) were observed along with a small amount of monomer (100 amu) due to unzipping reactions. C═C bonds along the main chain may have inhibited monomer emission by terminating unzipping reactions.

Another incubation phenomenon, particularly relevant to this study, was observed by Srinivasan *et al.* on PMMA exposed to 0.9 J/cm^2/pulse at 248 nm.[24] An initial swelling of the polymer surface was detected and attributed to the accumulation of gaseous products. They proposed that incubation involved the gradual buildup sufficient pressure to eject large polymer fragments.

Due to the importance of the 308 nm excimer laser for applications of laser ablation in industrial environments, an increasing number of studies at this wavelength have been published. A large variety of results and mechanisms have been reported. Threshold fluences vary from 0.2 to over 3 J/cm^2/pulse, and the etch patterns reveal rough features due to thermal effects.[10,11,25] Near the ablation threshold, photochemical processes may play an important role, although thermal processes may facilitate the creation of absorbers.[26] A similar conclusion was drawn from the ablation of PMMA with cw-Ar^+ lasers (351/363 nm). The existence of a power threshold, and the minor influence of the substrate material was used to argue that the temperature increase was only assisting in the restructuring of PMMA.[27]

To improve the ablation behavior, PMMA is often doped with various dyes. At 248 nm, dopants reduce the ablation threshold and increase the quality of ablated features.[28–30] In a recent review, it has been suggested that the ablation mechanism depends on the specific dopant/polymer/laser system.[31] Photolabile compounds generating gaseous products assist ablation by carrying ablation products away from the polymer. The photochemical properties of the dopants are also important.[32–34] Photostable dopants (e.g., polyaromatic compounds), can support photothermal, cyclic multiphoton mechanisms, where triplet states play a key role.[35] Pyrene, for example, can absorb at least 10 photons (at 248 nm) during a single laser pulse, converting this electronic energy to heat.[36] A temperature increase of $\sim$450 K has been calculated for surface swelling, and 700–1000 K for ablation.[37] Modifications of the polymer were responsible for incubation behavior.

Although numerous studies of PMMA ablation have been published, open questions about mechanisms remain. We reexamine the incubation process during irradiation at 308 nm at relatively low fluences and low dye (pyrene) concentrations. At these laser fluences, polymer vaporization dominates and is controllable, as opposed to explosive tearing of the material.[34,38] Likewise, critical changes induced in the PMMA by thermal and chemical processes initiated by the dopants can be more readily detected under these more controlled conditions. Further, these changes are slow enough to be monitored from pulse to pulse. We show that a common solvent [chlorobenzene (CB)] significantly enhances the laser ablation of PMMA under these conditions where we find vaporization/ablation to be principally photothermal.

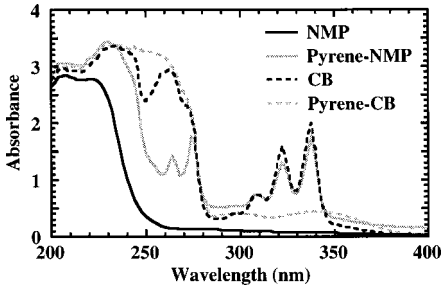

FIG. 1. Absorption spectra of PMMA samples: neat-NMP, pyrene-NMP, neat-CB, and pyrene-CB PMMA samples.

II. EXPERIMENT

A. Sample preparation and characterization

PMMA films were cast from medium molecular weight PMMA powder (M_w 120 000) using HPLC grade *N*-methyl 2-pyrrolidinone (NMP) and chlorobenzene (CB) as solvents. These films are designated NMP- and CB-PMMA, respectively. Pyrene-doped (0.1% by weight) films were cast using each solvent, and are designated with the prefix ''pyrene.'' This pyrene concentration is much smaller than the 1–5 wt % concentrations employed in most ablation studies. The mixture of polymer, solvent, and dye was covered and stirred at low heat (50 °C) for six hours. The solution was then poured into a mold and held at 76 °C for twelve hours. The resulting films were typically 100–400 μm thick.

Films containing pyrene and CB show distinctive features near 308 nm, as shown in Fig. 1. The 308 nm absorption band of pyrene is readily observed in pyrene-NMP-PMMA and pyrene-CB-PMMA. CB-PMMA displays significant absorption at 308 nm due to bands at $\sim$300 and $\sim$340 nm. This absorption is not intrinsic to CB; these bands may involve cage interactions, as discussed by Ouano and Pecora.[39] We estimate the residual CB concentrations to be on the order of 20 wt %. Lower concentrations are difficult to attain in PMMA due to slow CB outgassing in this concentration range.[40] Residual NMP in the NMP-PMMA samples does not significantly enhance absorption at 308 nm.

B. Experimental geometry

The experimental arrangement has been described in detail elsewhere.[41] Except where otherwise noted, all laser experiments were conducted in a diffusion-pumped, liquid-nitrogen trapped vacuum chamber at a pressure below

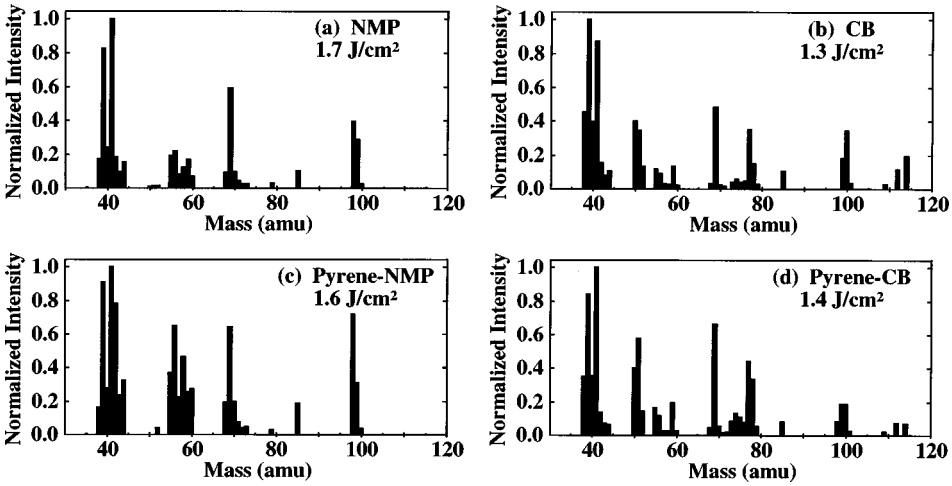

FIG. 2. Mass spectra of neutral emissions under steady-state conditions from (a) NMP-PMMA irradiated at 1.7 J/cm^2/pulse; (b) CB-NMP irradiated at 1.3 J/cm^2/pulse; (c) pyrene-NMP-PMMA irradiated at 1.6 J/cm^2/pulse; and (d) pyrene-CB-PMMA irradiated at 1.4 J/cm^2/pulse.

10^{-5} Pa. The beam from an excimer laser with a 30 ns pulse length operating at 308 nm (XeCl) and a pulse repetition rate of 1 Hz was directed onto the sample through a focusing lens (114 cm focal length) and mask. At a repetition rate of 1 Hz, accumulative heating in the PMMA is negligible. The fluence at the sample was controlled by adjusting the lens-to-sample distance, while a mask was used to control the laser spot size on the sample. The total laser energy density per pulse (fluence) used in this work ranged from 0.1 to 5 J/cm^2/pulse.

UV-visible absorption spectra were obtained before and after sample exposure at 308 nm. Transmission at 308 nm was also measured *in situ*, monitoring the transmitted energy as a function of laser exposure.

Neutral molecule mass spectra were obtained with a quadrupole mass spectrometer (QMS) using an electron impact ionizer operated at 70 eV and 2 mA emission. The temperature of neutral emission products (T) was determined by fitting the QMS arrival times to a Maxwell–Boltzmann distribution using nonlinear curve fitting techniques.[42] (Note that T represents the temperature of the source for a ''beam'' of effusing neutrals.) The Maxwell–Boltzmann time-of-flight (TOF) distribution is determined by transforming the velocity distribution for effusing particles to a spatial (density) distribution and integrating over the detection volume of the QMS ionizer. This procedure accounts for the fact that fast neutral particles spend less time in the ionizer volume than slow particles, and are therefore less likely to be ionized and contribute to observed signal. Assuming that emission is confined to the duration of the laser pulse, the number of molecules in the ionizer as a function of time, $A(t)$, is given by

$$A(t)=N_0\left(\frac{m}{kTt^2}\right)^2\int_D^{D+S} x\,\exp\left(\frac{-mx^2}{2kTt^2}\right)dx, \tag{1}$$

where t is the time after the laser pulse, m is the molecular mass, k is the Boltzmann constant, T is the temperature, D is the distance from the sample to the tip of the ionizer (17 cm), and S is the length of the ionizer (2 cm). N_0 is an adjustable parameter proportional to the total number of emitted particles, the efficiency of the ionizer, and the cross sectional area of the ionizer. The only other adjustable parameter is T, which controls the peak position and shape. Prior to analysis, the experimental TOFs were corrected for the transit time in the mass filter. Knudsen layer effects can be ignored due to the low density of gases generated at the fluences used here;[43] significant Knudsen layer effects are readily detected by their effect on the shape of the TOF curves. Fits were performed only on the first 500 μs of data to avoid signals due to particles which have bounced off vacuum system walls. With a beam block between the sample and QMS ionizer, detectable signals due to particles reaching the detector via indirect paths were not observed during the first 500 μs after the laser pulse. We see no evidence at these fluences that diffusion or gas phase collisions are contributing to the TOF shapes: all the gases appear to be coming off of the surface at approximate constant temperatures.

III. RESULTS

A. Identity of neutral emissions

Figure 2 shows the mass spectra of neutral products detected during low fluence irradiation of the four sample types. Each spectrum was acquired after incubation, during ''steady state'' emission. Table I lists the major emission peaks with our parent (source) species assignments. The strong signals at 41 and 99 amu are significant cracking fragments of both NMP and PMMA and cannot be unambiguously assigned. No pyrene-derived emissions were observed from pyrene-containing samples, presumably due to the low pyrene concentrations (0.1%). Molecular pyrene[44,45] and anthracene[46] have both been observed among the ablation products from PMMA containing these dyes.

The four mass spectra in Fig. 2 show similar PMMA derived peaks, although the relative intensities change somewhat with fluence. Overall, these changes reflect a trend toward the emission of lighter products (MMA fragments) at higher fluences. For instance, at low fluences, virtually all of the signal at 39 amu can be attributed to the fragmentation of MMA (100 amu) in the QMS ionizer. This is readily evident in the TOFs of the two species. At low fluences (<1 J/cm^2/pulse), the TOF signals for 100 and 39 amu peak at

TABLE I. Ion masses and assigned parent species.

Mass to charge ratio	Assigned parent species
(amu/e)	
39	Primary cracking fragment of PMMA monomer; Neutral $CH_2{=}C{=}CH$ as a decomposition product
41	Primary cracking fragment of PMMA monomer (unambiguous in samples not containing NMP)
44	Distinct NMP cracking fragment
50,51	Distinct chlorobenzene cracking fragment
55,56	Distinct PMMA cracking fragment
59	Primary cracking fragment of methyl formate (60 amu) ($COOCH_3$ as decomposition product of PMMA)
69	Distinct PMMA cracking fragment, $CH_2{=}C(CH_3)C{=}O$ as a decomposition product
77	Distinct chlorobenzene cracking fragment ($C_6H_5^+$)
85	Distinct PMMA cracking fragment
98	NMP minus H
99	PMMA monomer minus H or NMP molecule parent (unambiguous in samples not containing NMP)
100	PMMA monomer parent
112,114	Chlorobenzene molecule parent

very similar times. If both species were being emitted directly from the surface, the lighter particles should arrive before the heavier ones.

At higher fluences (>1 J/cm^2/pulse), the 39 amu signal peaks well before the 100 amu signal; further, the 39 amu signals at high fluences are much more intense relative to the 100 amu signals. This change indicates that the great majority of the 39 amu product, namely $CH_2{=}C{=}CH$, is being emitted directly from the sample and therefore (at high fluences) represents a product of laser-induced decomposition. With the exception of solvent-derived peaks, all samples yield similar mass spectra in the low fluence limit, and show similar changes as the fluence is raised. Thus the same decomposition mechanisms operate in all samples—including those with pyrene.

B. Neutral emission intensities during incubation

Over a wide range of laser fluences, neutral emission intensities at 308 nm do not exhibit a simple fluence threshold, but rather show incubation behavior. At low fluences (e.g., 0.9 J/cm^2/pulse) no MMA monomer emission is detected during the first few laser pulses. Figure 3 shows typical TOF curves for emission at 39 amu (the primary cracking fragment of MMA) at three points in the incubation process. After ten laser pulses, emission is still negligible. After 19 laser pulses, weak emissions are observed. Soon after the onset of emission, the intensity increases dramatically, as shown for the 29th laser pulse in Fig. 3. This behavior was observed at all fluences above 0.2 J/cm^2/pulse. Below this fluence, neutral emission intensities were negligible after 10^3 pulses; above this fluence, neutral emissions were observed after tens of pulses, and eventually displayed the dramatic increase in intensity which we associate with incubation.

During incubation, the transmission of laser light through the sample decreases markedly. Figure 4 illustrates the decrease in transmission with increasing number of laser

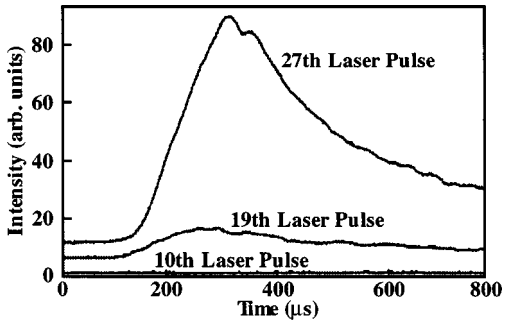

FIG. 3. Time-of-flight signals accompanying the 10th laser pulse (before the onset of significant neutral emission), the 19th laser pulse (just after the onset of significant neutral emission), and the 27th laser pulse (steady state emission).

pulses for CB-PMMA at a fluence of 2.0 J/cm^2/pulse. The total transmission decreases until the onset of intense neutral emission (after about 10 laser pulses at this fluence) and remains constant during steady-state neutral emission. Similar effects have been previously reported for irradiation at 248 nm.[21] Scanning electron microscopy (SEM) photographs of incubated areas show no crazing or blistering prior to the onset of neutral emission; therefore the drop in transmission is not due to surface roughening.

UV-VIS absorption spectra of pyrene-NMP-PMMA and CB-PMMA before and after 500 laser pulses at the subablative fluence of 0.20 J/cm^2/pulse confirm a buildup of near-UV/blue absorption, significantly decreasing transmission at 308 nm. The growth of absorption in this region is accompanied by a visible yellowing of the material. These changes are consistent with the formation of C═C double bonds and conjugated double bond systems.[22] In contrast, the pyrene bands at 322 and 338 nm in pyrene-containing samples decrease during laser exposure. Pyrene is expected to be stable under these conditions, suggesting that this decrease is not due to decomposition.[36,37] In this work, pyrene may have diffused to the surface and vaporized. The low pyrene concentration in these samples (0.1 wt %) would account for its absence from the mass spectra. The absence of pyrene-related features in the absorption spectra after incubation suggests that pyrene plays only a minor role during steady state ablation at low fluences. Nevertheless, the presence of

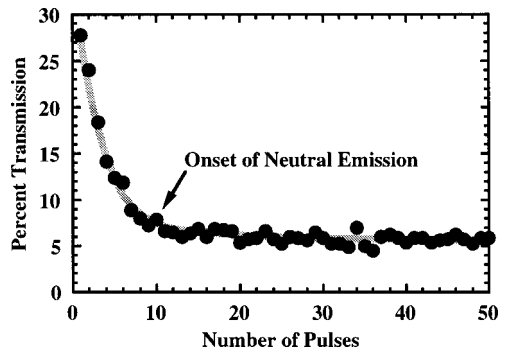

FIG. 4. Transmission of laser light (308 nm) through a typical CB-PMMA sample during successive laser pulses at a fluence of 2.0 J/cm^2/pulse.

TABLE II. Incubation parameters of samples.

Specimen type	Fluence	No. of incubation pulses	Dose
NMP-PMMA	2.9 J/cm^2/pulse	70 pulses	203 J/cm^2
pyrene-NMP-PMMA	0.9 J/cm^2/pulse	70 pulses	63 J/cm^2
CB-PMMA	0.7 J/cm^2/pulse	100 pulses	70 J/cm^2
pyrene-CB-PMMA	0.7 J/cm^2/pulse	85 pulses	59.5 J/cm^2
CB-PMMA (abraded)	0.2 J/cm^2/pulse	70 pulses	14 J/cm^2

pyrene *during incubation* strongly effects the steady state emission intensities, as shown below.

In contrast to PMMA containing CB or pyrene, NMP-PMMA showed no increase in absorption at 308 nm during prolonged irradiated at fluences as high as 0.5 J/cm^2/pulse. This is consistent with the lower sensitivity of NMP-PMMA to 308 nm irradiation. At higher fluences (>1 J/cm^2/pulse), NMP-PMMA does eventually display incubation behavior, including an increase in absorption at 308 nm. NMP-PMMA, with its low absorption at 308 nm, most closely represents the response of ''clean'' or ''undoped'' PMMA.

The number of incubation pulses (N_i) required to initiate measurable neutral emission (e.g., at 100 amu) is a strong function of laser fluence and sample type. The first four entries in Table II show the minimum fluence necessary to incubate each type of sample over a similar range of $N_i = 85 \pm 15$. Note the dramatic difference between NMP-PMMA and the other three sample types. Under these conditions, the NMP-PMMA samples require fluences at least three times higher than the other samples for incubation.

Figure 5 shows N_i versus fluence for each sample type for fluences ranging from 0.5 to 5 J/cm^2/pulse. Two different behaviors can be observed:

(1) Roughly power-law behavior for both NMP-PMMA and pyrene-NMP-PMMA, and for pyrene-CB-PMMA;
(2) More complex behavior for CB-PMMA, similar to pyrene-NMP-PMMA and pyrene-CB-PMMA at low fluences, but slower incubation (higher N_i) at high fluences.

In summary, the NMP-PMMA samples are much more difficult to incubate than the other samples, whereas PMMA with either pyrene or CB is much easier to incubate. Further, the presence of 0.1 wt % pyrene further facilitates incubation

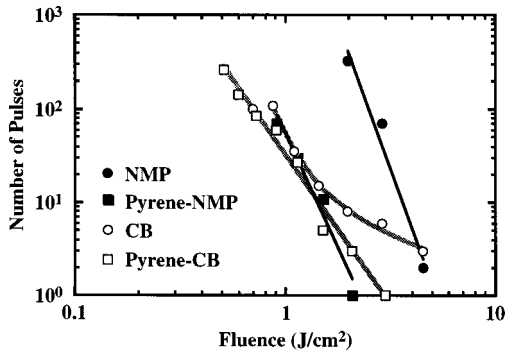

FIG. 5. Number of pulses required to initiate incubation as a function of fluence for NMP-PMMA, CB-PMMA, pyrene-NMP-PMMA, and pyrene-CB-PMMA.

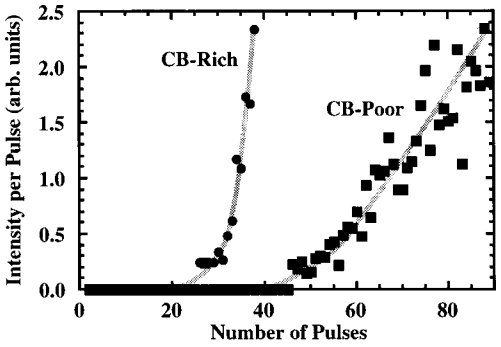

FIG. 6. Intensity of the 39 amu signal accompanying successive laser pulses from CB-rich and CB-poor pyrene-CB-PMMA irradiated at 1.2 J/cm^2/pulse.

in the CB-PMMA at the high end of the fluence range studied. (We caution that power law behavior under these conditions cannot be unambiguously be interpreted in terms of photoelectronic processes. For instance, thermally activated processes can yield very nearly power-law behavior over similar fluence ranges.)[47]

The effect of CB is readily verified by purposefully comparing solvent-rich and solvent-poor samples, where the solvent concentration is altered by shortening or lengthening the annealing stage of sample preparation as desired. Figure 6 shows the MMA emission from pyrene-CB-PMMA during incubation as a function of the number of laser pulses at 1.2 J/cm^2/pulse—a fluence where 0.1 wt % pyrene has little effect on the incubation of CB-containing PMMA. Emission from the CB-rich material begins after about 23 pulses, corresponding to a dose of about 27 J/cm^2. In contrast, emission from the CB-poor material required about 47 pulses, corresponding to a dose of about 56 J/cm^2. At this fluence, a high CB concentration clearly facilitates incubation.

Significantly, the neutral emission TOF signals shift to longer times over the course of incubation. This behavior is evident in Fig. 3, and can be quantified by fitting the observed TOF signals to Maxwell–Boltzmann velocity distributions. Figure 7 shows typical TOF signals for monomer emission (100 amu) from CB-PMMA at two stages of the induction process at a fluence of 0.9 J/cm^2/pulse. Figure 7(a) shows the emission from one of the first pulses yielding measurable emission (19th laser pulse), while Fig. 7(b) shows the TOF signal accompanying the 50th laser pulse on the sample. The temperature corresponding to the best fit was $\sim$1750 K for the 19th laser pulse, but only $\sim$840 K for the 50th laser pulse. A similar analysis of TOF signals at 112 amu (a CB-derived peak) under the same conditions gave very similar temperatures, both near the onset of emission ($\sim$1790 K) and at the onset of steady-state emission ($\sim$650 K). Thus the cooling effect is robust. The steady-state temperatures are similar to those determined in other studies.[15,16]

Since the progress of incubation corresponds to an increase in laser absorption and emission intensity, it is at first glance surprising that incubation is accompanied by a decrease in the effective temperature of the emitted products. Further insight into the cause of this ''cooling'' effect was obtained by SEM of typical PMMA surfaces before and after incubation.

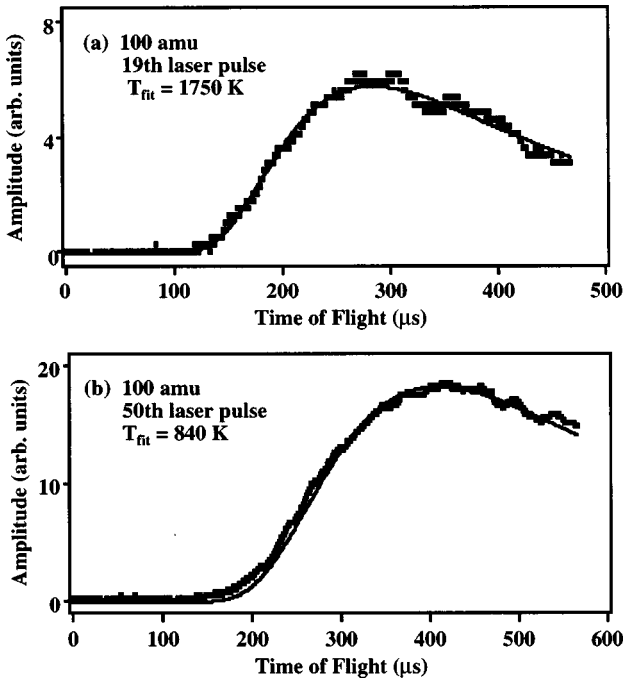

FIG. 7. Time-of-flight signals at 100 amu accompanying (a) the 19th laser pulse (near the onset of significant neutral emission) and (b) the 50th laser pulse (steady state emission) for CB-PMMA irradiated at 0.9 J/cm^2/pulse. The dark lines represent best-fit Maxwell–Boltzmann TOF distributions corresponding to 1750 K in (a) and 840 K in (b).

C. Surface morphology changes during incubation

The onset of neutral emission (at significant intensities) is accompanied by a marked change in the microscopic appearance of the surface (surface morphology). SEM images of CB-cast surfaces irradiated at 3.0 J/cm^2/pulse are shown in Fig. 8. Irradiation was terminated immediately after the onset of neutral emission in Fig. 8(a) (after two pulses), and soon after the saturation of neutral emission intensities in Fig. 8(b) (after four pulses). Prior to the onset of neutral emission, SEM images shown signs of subsurface swelling. The onset of neutral emission coincides with the appearance of disrupted material, reflecting the rupture of a relatively impermeable ''skin'' by gaseous products generated in the bulk. Solvent evaporation after casting can form a relatively impermeable skin by reducing the solvent concentration in the near-surface region. Since these solvents are effective plasticizers, material with high solvent concentrations (the bulk) is more flexible and permeable than material with low solvent concentrations (the surface layer). Volatile products created below the surface are thus trapped under the less permeable skin. After incubation is complete (emission saturates), the surface shows extensive cracking, as shown in Fig. 8(b).

This impermeable surface layer must be ruptured before significant neutral emission signals are detected. In many cases, disruption involves melting instead of fracture. Figure 9 shows the surfaces of neat NMP-PMMA samples exposed to (a) 10 (immediately after the onset of neutral emission) and (b) 20 laser pulses (during steady state emission) at 3 J/cm^2/pulse. Again, the image taken immediately after the onset of neutral emission shows surface swelling with a small ruptured area, but in this case the ruptured portion

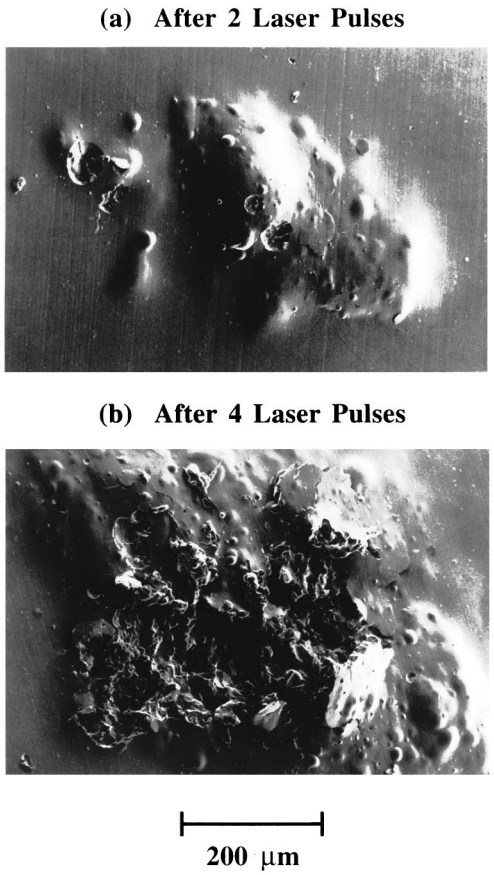

FIG. 8. SEM images of CB-PMMA surfaces exposed to 3.0 J/cm^2/pulse after (a) two laser pulses (immediately after the onset of neutral emissions) and (b) four laser pulses (steady state emission).

looks melted, rather than fractured. Surface melting resulting in rupture is typical of all four sample types at high fluences. This topography is characteristic of PMMA ablation at 248 nm as well, and has been previously reported.[25,34] Continuing irradiation until ''steady state'' emission is achieved producing large melted features, as shown in Fig. 9(b).

As a qualitative test of the influence of this outer layer, we removed patches of the surface layer of CB-PMMA samples by gentle abrasion with 400 grit sandpaper, removing the debris from the surface with several blasts of dry air. Comparing monomer neutral emission from abraded and unabraded CB-PMMA, Table II shows that vaporization of abraded samples starts at extremely low fluences, about 0.2 J/cm^2/pulse for $N_i = 73$ pulses. SEM photographs show similar surface cracking accompanies the onset of ablation for both abraded and unabraded surfaces; the primary difference between the two surfaces is that fissures are smaller and more uniform on the abraded surface. Mechanical abrasion weakens the skin at a number of places, allowing fracture at lower subsurface pressures and detectable neutral emission signals at lower fluences. Thus the onset of measurable particle emission is critically controlled by the breakup of the outer surface layer. At this point the exposed material has a high density of absorption centers which have remained in place due to the skin; thus, the temperature of the newly exposed laser heated surface is high. For the next few pulses

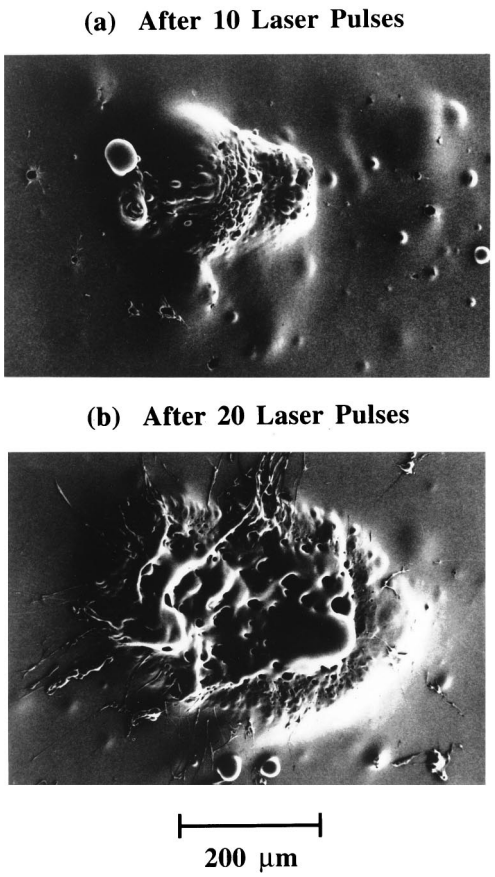

FIG. 9. SEM images of NMP-PMMA surfaces exposed to 3.0 J/cm^2/pulse after (a) ten laser pulses (immediately after the onset of neutral emissions) and (b) 20 laser pulses (steady state emission).

we therefore observe hotter gases (e.g., corresponding to a source temperature, $T_{surface}$, ~1750 K). With subsequent pulses, this highly absorbing material is removed resulting in a reduced surface temperature and correspondingly cooler gaseous emissions (e.g., corresponding to a $T_{surface}$~840 K).

We note that surface roughening can in principle enhance laser absorption in the near surface region. This effect has been observed in SiO_2,[48] where no ''impermeable surface layer'' exists. Abrasion can enhance the ablation of SiO_2 and similar materials by enhancing local electric fields near cracks and asperities,[49,50] or by forming absorbing point defects.[51–53] Although these effects are potentially active in PMMA, the structures revealed by SEM are more consistent with the disruption of an impermeable surface layer by the accumulation of subsurface volatiles.

D. Neutral emission intensities during steady state ablation

Following incubation, the neutral emission signals gradually plateau and remain relatively constant over a large number of pulses (steady state emission). The emission intensities at 39 amu (a primary PMMA cracking fragment) during steady state ablation is displayed for the four sample compositions as a function of fluence in Fig. 10. Samples prepared with CB yield more intense emissions at all fluences relative to samples prepared with NMP. At fluences

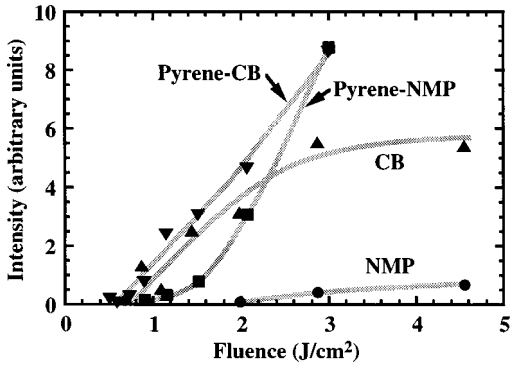

FIG. 10. Steady state emission intensities at 39 amu as a function of fluence for NMP-PMMA, CB-PMMA, pyrene-NMP-PMMA, and pyrene-CB-PMMA.

below 2 J/cm^2/pulse, the signal intensities from pyrene-CB-PMMA samples are quite similar to the sum of the intensities from CB-PMMA and pyrene-NMP-PMMA, suggesting that the effect of CB and pyrene is additive at these fluences. At fluences below 1.5 J/cm^2/pulse, the presence of CB has a much greater effect on yield than the presence of pyrene. But as the fluence is raised above 1.5 J/cm^2/pulse, emission from pyrene containing samples increases dramatically—surpassing that of CB-PMMA at 2.3 J/cm^2/pulse. At still higher fluences, the effect of pyrene dominates that of CB. (The yield from pyrene-NMP is similar to the yield from pyrene-CB-PMMA—even at the low pyrene concentration of 0.1 wt %.) Above 3 J/cm^2/pulse, the signals from pyrene containing samples saturated our detectors. For the samples without pyrene, the emission levels plateau at fluence above 3 J/cm^2/pulse, with significantly higher emissions from CB-PMMA than from NMP-PMMA.

As in the case of the incubation, pyrene and CB at these concentrations act in an additive fashion. At low fluences, the role of CB is more pronounced, whereas at high fluences, pyrene dominates.

IV. DISCUSSION

The ablation of PMMA has been mainly studied at wavelengths below 300 nm. In the presence of appropriate absorption centers, PMMA can also be ablated at longer wavelengths. These absorption centers typically involve defects, either ''intrinsic,'' such as double bonds from chain end termination, or ''extrinsic,'' such as occluded solvents, particles from the environment, or impurities introduced during polymerization.[54] Photochemically, three general decomposition mechanisms have been observed:[55,56]

(1) Random homolytic scission of the polymer backbone, producing carbon radicals which can initiate unzipping reactions (=depolymerization).
(2) Photolysis of the methyl side chain, producing chain end C═C double bonds and radicals, which can again initiate polymer unzipping.
(3) Photolysis of the ester side group, diagrammed schematically in Fig. 11. This is the most important reaction at wavelengths longer than 230 nm, including 308 nm.

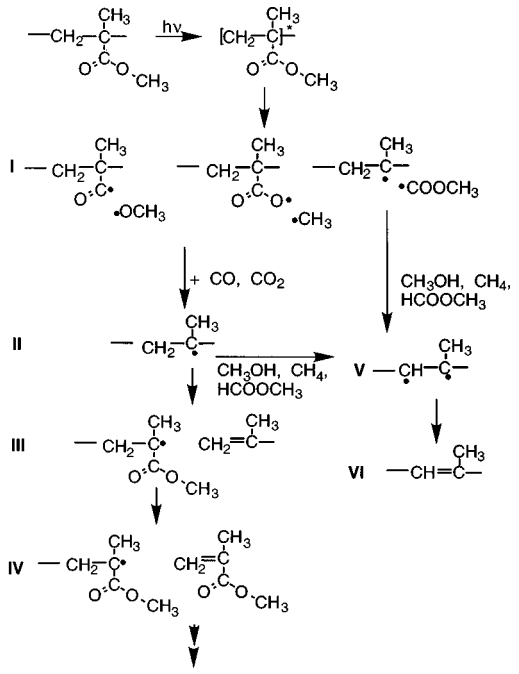

FIG. 11. Photolysis of the ester side chain: (I) Small radicals formed by ester photolysis; (II) abstraction of CO and CO_2 to form main chain C radical; (I)→(V) and (II)→(V) hydrogen abstraction to form small molecular fragments; (III) chain scission and the formation of a chain-end C=C double bond and an MMA radical; (IV) photochemical and/or low activation energy, thermally activated unzipping to release MMA; and (VI) the subsequent formation of a main-chain C=C double bond.

Photolysis of the ester side group often yields small radicals (Step I in Fig. 11), such as the methoxy, methyl, and methyl formate radicals. These radicals abstract hydrogen from the remainder of the chain to form CH_3OH, CH_4, $HCOOCH_3$, common products of PMMA photolysis which serve as ''indicators'' of ester group photolysis. Hydrogen abstraction from the polymer chain (Steps V–VI in Fig. 11) also produces main chain double bonds, which enhance laser absorption and provide vulnerable sites for the initiation of thermal unzipping. Small radicals can also inhibit unzipping reactions by recombining with chain-end radicals. Photolytic removal of the entire ester group (Step II in Fig. 11) creates a carbon chain radical and two other typical photolytic products, CO and CO_2; this radical can further react to form a chain end C═C double bond and another chain radical (Step III). Thermal unzipping, illustrated in Step IV, yields the monomer, methylacrylate (MMA). A variety of experiments have confirmed that PMMA photolysis at wavelengths longer than 240 nm generates gaseous molecules (CH_3OH, CH_4, $HCOOCH_3$, CO, and CO_2), and that the associated chain radicals are quickly destroyed by reactions with small radicals.[56] FTIR spectroscopy has also revealed an important aldehyde (H-C═O) product.[56]

The ability of 308 nm radiation to photolyze the ester side group in intrinsic PMMA presumably depends on the long wavelength absorption tail of the relevant electronic transition. Incubation both increases the absorption at 308 nm and the photoproduct intensities. The enhanced absorption at 308 nm is typically attributed to C═C double bonds (along the chain and at chain ends), and this absorption presumably promotes photolysis of the ester side group as well. In any case, the thermal, photochemical, or chemical processes which conjugate bonds also enhance subsequent photochemical generation of C═C structures.

Once these C═C structures are created, they also promote subsequent thermal unzipping, which nearly exclusively yields MMA from polymer unzipping (''depolymerization''). An important parameter for thermal decomposition is the ceiling temperature, T_c. Under equilibrium conditions, assuming reversible polymerization and depolymerization, the polymer concentration will decrease with increasing temperature: T_c is the temperature at which the polymer concentration ''goes to zero.'' For PMMA, $T_c \sim 550$ K. ''Distillation'' of PMMA at T_c can be used to produce ultraclean MMA. Time-of-flight temperatures of MMA and MMA fragments during induction and steady state emission are significantly higher, consistent with a depolymerization reaction. The short duration of the laser pulse limits the amount of product produced in the accompanying thermal spike. Thus substantially higher temperatures are usually required to produce significant thermal emissions.

In atactic PMMA, the standard product of radical polymerization, two thermal reactions have been identified.[57]

(1) A fast reaction initiated at chain end double bonds, resulting in unzipping.
(2) A slower reaction, with a higher activation energy, initiating at random points along the polymer backbone, which also results in unzipping.

Combining the photochemical and thermal decomposition pathways, the following overall mechanism can be derived. Photochemical reactions create C═C double bonds which increase UV absorption and facilitate further photochemical decomposition. These chain end double bonds are initiation sites for low activation energy thermal decomposition (unzipping—Reaction 1 above). The yield of unzipping reactions is a very strong function of temperature. Unzipping reactions which yield six monomer units per chain end radical at room temperature will yield 200 monomer units per chain end radical at 160 °C. Photochemical reactions can also be more efficient at higher temperatures:[58] the elevated temperatures which promote thermal decomposition can also accelerate photochemical decomposition. The interaction of the two decomposition mechanisms result in positive feed back. Both photochemical and photothermal mechanisms are important in this work, as indicated by the photoyellowing of the sample, the presence of typical photoproducts (e.g., methyl formate), the presence of the important thermal product MMA, and the temperatures derived from the TOF measurements (in a reasonable range for thermal decomposition).

Although CB and pyrene both enhance bond conjugation during incubation, they function in somewhat different manners, as suggested by contrasting induction behaviors (Fig. 5) and steady state emission intensities (Fig. 10).

Chlorobenzene may play a variety of roles in the ablation of PMMA. As shown in Fig. 1, the presence of CB enhances absorption at 308 nm; which can promote both photochemical and photothermal processes. Further, the photochemical decomposition of CB produces very reactive phe-

nyl and chorine radicals. These radicals are expected to abstract hydrogen from the polymer chain to produce C═C bonds, further increasing absorption at 308 nm and providing initiation sites for unzipping. CB is also quite volatile, boiling at 132 °C; this is well below the temperatures at which PMMA decomposes thermally (⩾277 °C). As the peak temperatures rise during incubation, CB vapor could contribute significantly to the ''pressure'' exerted by gaseous species on the thin PMMA skin produced by solvent casting. This would facilitate surface rupture and thus accelerate incubation as defined in this work. Thus CB can have three functions: (a) increasing absorption to support photochemical and photothermal processes, (b) forming chain end C═C bonds via reactions with phenyl and chlorine radicals, and (c) contributing directly to the pressure that ruptures the surface skin. The latter two processes can operate at relatively low temperatures, promoting fracture of the surface skin (in Fig. 8 for CB-PMMA) as opposed to melting (in Fig. 9 for NMP-PMMA) during incubation at modest and low fluences.

Pyrene is a common dopant in polymer laser ablation.[59–63] A general mechanism has been suggested for the role of polyaromatic dopants, such as pyrene, in the laser ablation of PMMA.[35] Pyrene and similar dopants are capable absorbing photons and deexciting nonradiatively in a fashion that heats the PMMA matrix without destroying the dopant.[59] The proposed cyclic, single photon absorption begins with excitation from the singlet ground state, S_0, to one of a number of higher states, S_1-S_n. These excited states rapidly undergo internal conversion to the S_1 state; an intersystem crossing subsequently produces a long-lived excited triplet state (T_1). The T_1 state can be repeatedly excited to a higher state, T_m, which decays by internal conversion to the T_1 state. This cyclic excitation and decay can take place several times (up to 10) during one excimer laser pulse (30 ns), thereby efficiently heating the matrix. This process can strongly enhance the thermal decomposition of PMMA.

Absorption measurements indicate that little pyrene remains in fully inducted samples prepared with pyrene. Since pyrene is expected to be stable over this range of fluences, we attribute this depletion to diffusion to the surface and subsequent vaporization. Nevertheless, steady state emission from these samples at high fluences is much more intense than samples prepared without pyrene (Fig. 10). During induction, the combination of high fluence irradiation and pyrene produces a persistent and effective change in sample chemistry that allows for sustained emission after the depletion of pyrene. The simplest change consistent with absorption measurements is the formation of high densities of C═C structures. The resulting steady state emissions can be sustained for many thousands of laser pulses. These emissions include CO_2 and $COOCH_3$ (Fig. 2), expected products of ester side group photolysis. Carbon double bond formation is a common product of this reaction, and would provide a mechanism to replenish C═C bonds consumed during prolonged irradiation. Absorption at these and similar structures would heat the sample strongly and account for the intense thermal emission of MMA and MMA fragments.

Since CB and pyrene operate independently, it is not surprising that the samples with both dopants yield more intense emissions (Fig. 10). At low fluences, CB alone is much more effective than 0.1 wt % pyrene alone in promoting incubation (Fig. 5) and in enhancing steady state ablation after incubation (Fig. 10). At high fluences (>2–3 J/cm^2/pulse) the effect of pyrene dominates. This is consistent with cyclic, single photon absorption in pyrene, where the probability of multiple photon absorption events during a single laser pulse becomes significant only at higher laser fluences. We note that on a per molecule basis, pyrene is a much more effective dopant than CB. At higher pyrene concentrations, the role of CB would be relatively much smaller.

The other important role of the dopants and decomposition is the creation of small gaseous molecules which cause an increase of pressure inside the polymer and the subsequent mechanical rupture/fragmentation of the polymer. This mechanism is strongly influenced by sample preparation. Solvent cast films typically display a thin surface skin capable of trapping gaseous products inside the polymer. Vaporization of the solvent will also contribute to pressure buildup. The explosive rupture of this skin allows decomposition products to escape and sets the stage for the development of steady state emission. If the skin layer is damaged, e.g., by abrasion, emission of products starts much earlier.

V. SUMMARY AND CONCLUSION

PMMA doped with CB and/or pyrene is readily incubated and ablated at 308 nm. The neutral emissions from the solvent-cast samples employed in this work display an incubation effect which is inherent to the casting process. Solvent casting produces a thin skin that hinders the escape of small gaseous products produced during the early stages of irradiation. Few products are detected during this early stage. The accumulation of products beneath this skin leads to polymer swelling and eventually ruptures this skin. Subsequently, neutral emission accompanies every laser pulse.

At 308 nm, both pyrene and CB accelerate the production of C═C bonds along the polymer backbone during incubation. In the case of pyrene, bond conjugation is presumably due to photothermal effects. In the case of CB, hydrogen abstraction by products of photochemical photodecomposition presumably promotes bond conjugation. Although CB is by itself transparent at 308 nm, interactions with PMMA form new absorption centers (300 and 340 nm) that promote this photochemical incubation. At low fluences, the CB in our samples (~20 wt %) is more effective for incubation and ablation than 0.1 wt % pyrene. At fluences above 2–3 J/cm^2/pulse, the effect of pyrene dominates that of CB. Subsequent, steady state ablation is best described as a *(photo)thermal* process. The main ablation product is MMA and its fragments.

Conjugated bonds formed as the result of laser interactions with pyrene and CB-PMMA both promote *photochemical* reactions involving the ester side chain (methyl formate as product) which conjugate additional bonds. At the low pyrene concentrations used in this study, steady state ablation is reached and sustained even after the depletion of pyrene from the polymer film. Ablation of the remaining PMMA is sustained by interactions with C═C structures

generated during and after incubation. These double bonds serve two functions: (a) enhancing laser absorption and thus promoting further photochemical processes and laser-induced heating, and (b) providing initiation sites for unzipping reactions (thermal decomposition initiated at C═C bonds). The temperatures inferred from the TOF measurements are consistent with thermal decomposition. Therefore, we conclude that the monomer is a product of thermal and not photochemical reactions. Finally, the fact that CB and pyrene together are more effective than either dopant alone suggests that dopant combinations may be an effective way to improve the laser ablation of polymers.

ACKNOWLEDGMENTS

We thank Charles Davis, IBM Endicott, for helpful discussions. This work was supported by the Department of Energy, Office of Basic Energy Sciences-Division of Chemical Sciences under Contract No. DE-FG03-98ER14864.

[1] R. Iscoff, Laser and Optronics **6**, 65 (1987); M. Isner, P. G. Steg, and R. H. Clarke, IEEE J. Quantum Electron. **23**, 482 (1986); H. Nornes, R. Srinivasan, R. Solanski, and E. Johnson, Soc. Neurosci. Symp. **11**, 1167 (1985); R. J. Lane, R. Linsker, J. J. Wynne, A. Torres, and R. G. Geronemus, Arch. Dermatol. **121**, 609 (1985); Y. T. C. Yeh, J. Vac. Sci. Technol. A **4**, 653 (1986); S. Lazare and V. Granier, Laser Chem. **10**, 25 (1989); R. Srinivasan and B. Braren, Chem. Rev. **89**, 1303 (1989); P. E. Dyer, in *Photochemical Processing of Electronic Materials*, edited by I. W. Boyd and R. B. Jackman (Academic, London, 1992), p. 359.
[2] A. Gupta, R. Liang, F. D. Tsay, and J. Moacanin, Macromolecules **13**, 1696 (1980).
[3] R. Srinivasan, B. Braren, D. E. Seeger, and R. W. Dreyfus, Macromolecules **19**, 916 (1986).
[4] D. J. Krajnovich, J. Phys. Chem. A **101**, 2033 (1997).
[5] R. F. Cozzens and R. B. Fox, Polym. Eng. Sci. **18**, 900 (1978).
[6] R. C. Estler and N. S. Nogar, J. Vac. Sci. Technol. B **5**, 1465 (1987).
[7] R. C. Estler and N. S. Nogar, Appl. Phys. Lett. **49**, 1175 (1986).
[8] G. B. Blanchet and C. R. Fincher, Jr., Appl. Phys. Lett. **65**, 1311 (1994).
[9] G. B. Blanchet and C. R. Fincher, Jr., Adv. Mater. **6**, 881 (1994).
[10] M. Tsunekawa, S. Nishio, and H. Sato, J. Appl. Phys. **76**, 5598 (1994).
[11] M. Tsunekawa, S. Nishio, and H. Sato, Jpn. J. Appl. Phys., Part 1 **34**, 218 (1995).
[12] D. E. Hare and D. D. Dlott, Appl. Phys. Lett. **64**, 715 (1994).
[13] D. E. Hare, J. Franken, and D. D. Dlott, J. Appl. Phys. **77**, 5950 (1995).
[14] B. Danielzik, N. Fabricius, M. Röwekamp, and D. von der Linde, Appl. Phys. Lett. **48**, 212 (1986).
[15] G. M. Davis, M. C. Gower, C. Fotakis, T. Efthimiopoulos, and P. Argyrakis, Appl. Phys. A: Solids Surf. **36**, 27 (1985).
[16] G. C. D'Couto and S. V. Babu, J. Appl. Phys. **76**, 3052 (1994).
[17] R. Srinivasan, B. Braren, and K. G. Casey, Pure Appl. Chem. **62**, 1581 (1990).
[18] G. M. Davis and M. C. Gower, J. Appl. Phys. **61**, 2090 (1987).
[19] A. K. Baker and P. E. Dyer, Appl. Phys. A: Solids Surf. **57**, 543 (1993).
[20] J. Meyer, J. Kutzner, D. Feldmann, and K. H. Welge, Appl. Phys. B: Photophys. Laser Chem. **45**, 7 (1988).
[21] S. Küper and M. Stuke, Appl. Phys. A: Solids Surf. **49**, 211 (1989).
[22] S. Lazare, J. Lopez, J.-M. Turlet, M. Kufner, S. Kufner, and P. Chavel, Appl. Opt. **35**, 4471 (1996).
[23] R. Srinivasan and B. Braren, J. Appl. Phys. **68**, 1837 (1990).
[24] R. Srinivasan, B. Braren, and K. G. Casey, J. Appl. Phys. **68**, 1842 (1990).
[25] A. Costela, J. M. Figuera, F. Florido, I. Garcia-Moreno, E. P. Collar, and R. Sastre, Appl. Phys. A: Solids Surf. **60**, 261 (1995).
[26] H. Guo and Q. Lou, J. Appl. Phys. **70**, 2333 (1991).
[27] S. I. Bozhevolnyi, I. V. Potemkin, and V. B. Svetovoy, J. Appl. Phys. **71**, 2030 (1992).
[28] Y. Kawamura, K. Toyoda, and S. Namba, Appl. Phys. Lett. **40**, 374 (1982).
[29] R. Srinivasan, B. Braren, R. W. Dreyfus, L. Hadel, and D. E. Seeger, J. Opt. Soc. Am. B **3**, 785 (1986).
[30] H. Fujiwara, T. Hayashi, H. Fukumura, and H. Masuhara, Appl. Phys. Lett. **64**, 2451 (1994).
[31] T. Lippert, A. Yabe, and A. Wokaun, Adv. Mater. **9**, 1 (1997).
[32] J. Ihlemann, M. Bolle, K. Luther, and J. Troe, Proc. SPIE **1361**, 1011 (1990).
[33] B. R. Arnold and J. C. Scaiano, Macromolecules **25**, 1582 (1992).
[34] T. Lippert, J. Stebani, J. Ihlemann, O. Nuyken, and A. Wokaun, Angew. Makromol. Chem. **213**, 127 (1993).
[35] H. Fukumura and H. Masuhara, Chem. Phys. Lett. **221**, 373 (1994).
[36] H. Fujiwara, T. Hayashi, H. Fukumura, and H. Masuhara, Appl. Phys. Lett. **64**, 2451 (1994).
[37] H. Fukumura, N. Mibuka, S. Eura, and H. Masuhara, Appl. Phys. A: Solids Surf. **53**, 255 (1991).
[38] T. Lippert, J. Dauth, O. Nuyken, and A. Wokaun, in *Polymer-Solid Interfaces*, edited by J. J. Pireaux, P. Bertrand, and J. L. Bredas (IOP, Bristol, 1992), p. 391; T. Lippert, J. Stebani, J. Ihlemann, O. Nuyken, A. Wokaun, Angew. Makromol. Chem. **213**, 127 (1993).
[39] A. C. Ouano and R. Pecora, Macromolecules **13**, 1173 (1980).
[40] A. C. Ouano and R. Pecora, Macromolecules **13**, 1167 (1980).
[41] P. A. Eschbach, J. T. Dickinson, S. C. Langford, and L. R. Pederson, Appl. Phys. A: Solids Surf. **7**, 2943 (1989).
[42] J. T. Dickinson, J. Appl. Phys. **74**, 4729 (1993).
[43] R. Kelly and R. W. Dreyfus, Surf. Sci. **198**, 263 (1988).
[44] H. Fukumura, Y. Kohji, K.-I. Nagasawa, and H. Masuhara, J. Am. Chem. Soc. **116**, 10304 (1994).
[45] H. Fukumura, Y. Kohji, and H. Masuhara, Appl. Surf. Sci. **96–98**, 569 (1996).
[46] H. Fukumura, N. Mibuka, S. Eura, H. Masuhara, and N. Nishi, J. Phys. Chem. **97**, 13761 (1993).
[47] J. T. Dickinson, J.-J. Shin, and S. C. Langford, Appl. Surf. Sci. **96–98**, 326 (1996).
[48] J. Ihlemann, B. Wolff, and P. Simon, Appl. Phys. A: Solids Surf. **54**, 363 (1992).
[49] N. Bloembergen, Appl. Opt. **12**, 661 (1973).
[50] R. L. Webb, S. C. Langford, and J. T. Dickinson, J. Appl. Phys. **80**, 7057 (1996).
[51] J. Krüger and W. Kautek, Appl. Surf. Sci. **96–98**, 430 (1996).
[52] R. L. Webb, L. C. Jensen, S. C. Langford, and J. T. Dickinson, J. Appl. Phys. **74**, 2323 (1993).
[53] J.-J. Shin, M.-W. Kim, and J. T. Dickinson, Appl. Phys. **80**, 7065 (1996).
[54] J. F. Rabek, *Mechanism of Photophysical Processes and Photochemical Reactions in Polymers* (Wiley, Chichester, 1987).
[55] J. F. McKellar and N. S. Alden, *Photochemistry of Man-Made Polymers* (Applied Science, London, 1979).
[56] A. Gupta, R. Liang, F. D. Tsay, and J. Moacanin, Macromolecules **13**, 1696 (1980).
[57] H. H. G. Jellinek and M. D. Luh, Makromol. Chem. **115**, 89 (1968).
[58] J. L. Graham, J. M. Berman, and B. Dellinger, J. Photochem. Photobiol., A **71**, 65 (1993).
[59] H. Fujiwara, T. Hayashi, H. Fukumura, and H. Masuhara, Appl. Phys. Lett. **64**, 2451 (1994).
[60] H. Masuhara, H. Hiraoka, and K. Domen, Macromolecules **20**, 452 (1987).
[61] H. Hiraoka, T. J. Chuang, and H. Masuhara, J. Vac. Sci. Technol. B **6**, 463 (1988).
[62] T. J. Chuang, H. Hiraoka, and A. Moedl, Appl. Phys. A: Solids Surf. **45**, (1988).
[63] A. Itaya, A. Kurahashi, H. Masuhara, Y. Tanaguchi, and M. Kiguchi, J. Appl. Phys. **67**, 2240 (1990).